Using nanoscopic solvent defects for spatial and temporal manipulation of single assemblies of molecules

Soumik Das, ‡ [a] JungHyun Noh, ‡ [a] Wei Cao, [b] Hao Sun, [b][c] Nathan C. Gianneschi, \*[b] and Nicholas L. Abbott \*[a]

[a] School of Chemical and Biomolecular Engineering, Cornell University, Ithaca, New York 14853, United States

[b] Department of Chemistry, Materials Science & Engineering, Biomedical Engineering, Pharmacology, International Institute for Nanotechnology, Simpson Querrey Institute, Chemistry of Life Processes Institute and the Lurie Cancer Center, Northwestern University, Evanston, Illinois 60208, United States

[c] Department of Chemistry and Chemical & Biomedical Engineering, University of New Haven, West Haven, Connecticut 06516, United States

KEYWORDS: Nematic solvents, Self-assembly, Defects, Molecular transport, Assembly dynamics.

ABSTRACT: Here we report the use of defects in ordered solvents to form, manipulate and characterize individual molecular assemblies of either small-molecule amphiphiles or polymers. The approach exploits nanoscopic control of the structure of nematic solvents (achieved by introduction of topological defects) to trigger formation of molecular assemblies, and subsequent manipulation of defects using electric fields. We show that molecular assemblies formed in solvent defects slow defect motion in the presence of an electric field and that time-of-flight measurements correlate with assembly size, suggesting methods for characterization of single assemblies of molecules. Solvent defects are also used to transport single assemblies of molecules between solvent locations that differ in composition, enabling assembly and disassembly of molecular "nanocontainers". Overall, our results provide new methods for studying molecular self-assembly at the single assembly level and new principles for integrated nanoscale chemical systems that use solvent defects to transport and position molecular cargo.

The development of integrated micro- and nano-scale methods for the assembly, manipulation and characterization of complexes formed by amphiphiles and polymers underlies efforts to accelerate the discovery of new functional materials, drug formulations and consumer products.<sup>1–</sup> Examples of prior approaches include bead-based syntheses, <sup>1–3</sup> photochemical syntheses and the use of droplet-based microfluidic reactors.<sup>4–9</sup> Key challenges that underlie the realization of integrated micro- and nano-scale chemical systems include reagent manipulation (e.g., transport/transfer of molecules between solution environments), separation of reactants and products, as well as product characterization.<sup>4,10–12</sup> To this end, assemblies of amphiphiles and polymers, including lipid vesicles, <sup>13,14</sup> block copolymer assemblies, <sup>15–22</sup> and polyelectrolyte

complexes<sup>23–25</sup> have been exploited for localization of reagents and associated physicochemical processes (e.g., precipitation),<sup>13,17,18,20,21,23–30</sup>. The ultimate limit to the scaling down of such integrated processes is to work with single assemblies (i.e., single nano-containers). Reaching this limit, however, requires the development of methods for manipulation of single assemblies as well as methods that permit characterization at the single assembly level.<sup>31–35</sup>. The importance of scaling down synthesis and property measurement is growing as artificial intelligence/data-driven methods of discovery are demanding large datasets for the training of optimization algorithms.<sup>36–39</sup>

In this paper, we report the development of principles for manipulation and characterization of assemblies formed by amphiphiles and polymers at the single assembly level. We show that it is possible to move individual nano-scale assemblies of molecules between solvent environments that differ in composition. Such targeted placement of assemblies of molecules enables physical and chemical transformations (e.g., assembly and disassembly of "containers" to uptake and release reagents). We also show that it is possible to optically measure the motion of single assemblies of molecules in response to electric fields, providing principles for "time-of-flight" characterization methods for integration with single-assembly synthesis methods for chemical discovery.

The approach reported in this paper for the spatial and temporal manipulation of single assemblies of molecules relies on the careful choice of solvent, which is a critical decision in any chemical synthesis or manipulation in solution. 40–44 In this paper, we use nematic solvents, 45 solvents that possess long-range orientational ordering of the constituent molecules (Figure 1a-b). In contrast to water and other isotropic solvents, the long-range ordering of molecules in nematic solvents permits tailoring of solvent structure on the nanometer-scale by introduction of so-called

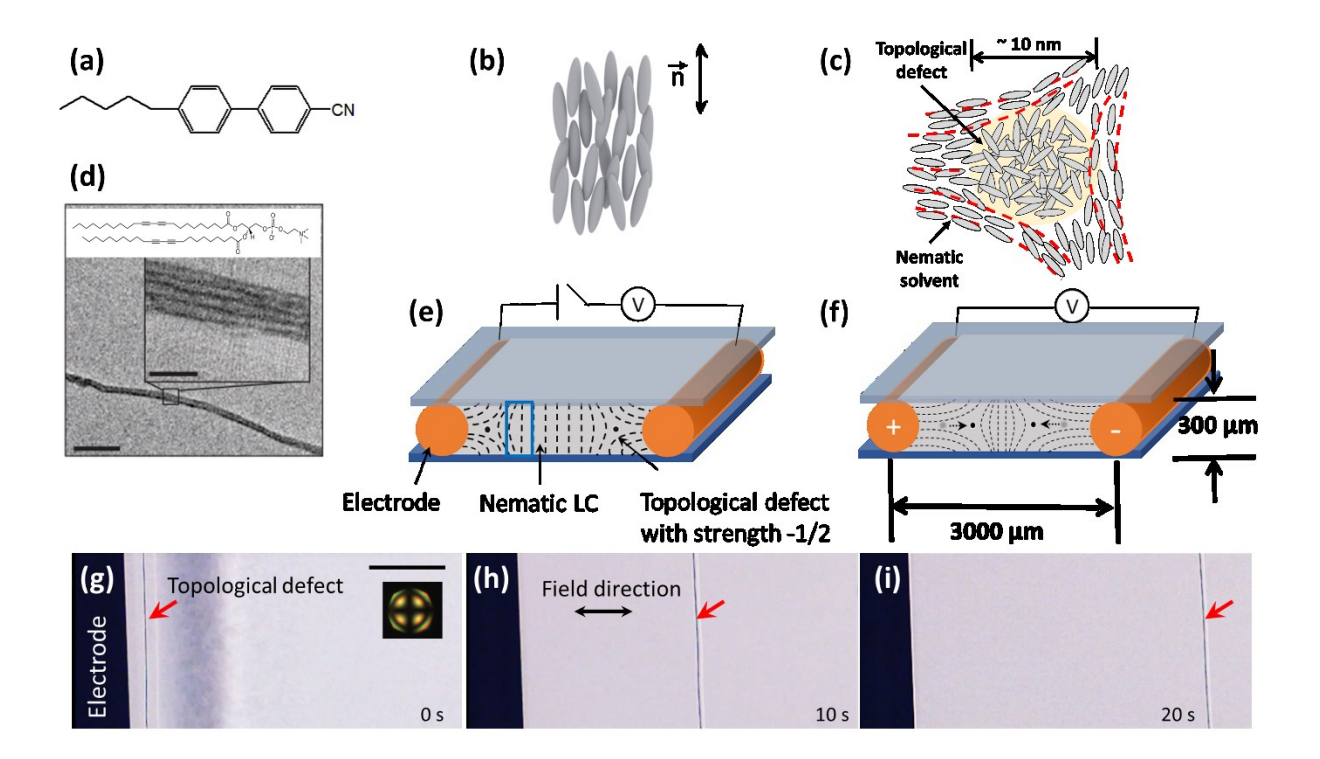


Figure 1. Molecular structure of (a) 4-cyano-4'-pentylbiphenyl (5CB) and (b) schematic illustration of molecular ordering in nematic solvent (the average orientation of molecules is indicated by  $\vec{n}$ , called the director). (c) Schematic illustration of the disordered solvent core of a m = -1/2 defect; the size of the core is ~10 nm. (d) TEM images of assemblies of 1,2-bis(10,12-tricosadiynoyl)-sn-glycero-3- phosphocholine (polymerizable lipid; inset of figure) formed in line defects of a nematic solvent phase of 5CB. Reproduced with permission. <sup>46</sup> Copyright © 2015, Nature Publishing Group. (e) Experimental set-up used to generate a pair of topological defects with strength m = -1/2 in nematic 5CB solvent and (f) displacement of defects in e) following application of the electric field. (g-i) Optical micrographs showing a defect moving away from the left electrode under the influence of an electric field. The time after which the electric field was applied (50V, 1kHz AC) is indicated. Inset in (g) shows a conoscopic image confirming uniform homeotropic orientation in the film of 5CB. Scale bar, 100 μm

topological defects.<sup>46–51</sup> Topological defects arise in nematic solvents when surface-imposed orientations frustrate the packing of solvent molecules, leading to nanoscopic regions of solvent with diminished levels of orientational order and high free-energy density (Figure 1c).<sup>45,52–54</sup>

Defects in nematic solvents can take the shapes of points,  $^{47,52}$  lines (disclinations)  $^{53,55,56}$  or walls,  $^{45,57}$  with the region of disordered solvent typically being about ~10 nm in size (e.g., diameter of a line defect). The high free energy density of the disordered solvent in the defect core has been

shown to trigger the formation of well-defined assemblies of both small-molecule amphiphiles and polymers at concentrations below which assemblies form in the bulk nematic solvent phase. 46,47,51,58,59 For example, dipyrrometheneboron difluoride (BODIPY) -labeled fatty acids (BODIPY-alkanoic acids) and phospholipids (e.g., 1,2-dilauroyl-sn-glycero-3-phosphocholine (DLPC))<sup>46</sup> undergo cooperative self-assembly in nematic solvent defects with thermodynamic signatures (e.g., critical aggregation concentrations) analogous to those observed with amphiphiles in aqueous solvent systems. Super-resolution optical microscopy (STORM) and cryo-transmission electron microscopy (cryo-TEM) reveal that the phospholipid amphiphiles formed multilamellar cylindrical assemblies with mean diameters of ~30 nm in line defects (Figure 1d), 46 or nanoscopic toroidal assemblies with overall diameters of 200 nm in point defects<sup>47</sup>. Additionally, assemblies of random copolymers of 2-hydroxyethyl methacrylate (HEMA) and 9-anthrylmethyl methacrylate (AnMA) form within line defects of nematic solvents, and after cross-linking by UV irradiation, possess worm-like morphologies with a mean diameter ~ 30 nm. <sup>51</sup> In contrast to prior studies of molecular self-assembly in aqueous solvents, solvents within which assemblies form at random locations, topological defects in nematic solvents enable formation of assemblies at predictable positions within the solvent. This represents a key advantage of using nematic solvents for manipulation of single assemblies of molecules, as explored in this paper.

We generated nanoscopic defects within nematic solvents using two copper wires to separate two glass slides (Fig. 1e; see SI). Upon filling the cavity with 5CB (Fig. 1a), line defects (strength m=-1/2; Figure 1c,e; see SI, Figure S4 for discussion regarding the strength of defects) were observed to form parallel to each wire, as evidenced by the dark lines in the bright-field optical image shown in Figure 1g. Figures 1g-i show the line defect at different times following application of 50V (1 kHz) between the copper wires. The defect is driven across the optical

sample cell (left to right) at a velocity of 17  $\mu$ m/s by the reorientation of the nematic solvent under the influence of the electric field (see Figure 1f).<sup>60</sup> Upon removal of the applied voltage, the line defect in the nematic solvent relaxed back to its initial location.

Next, we filled optical cells of the type described above with 5CB containing fatty acids (with C5 and C12 tails) conjugated with BODIPY (BODIPY-C5 and BODIPY-C12; Fig 2a) to determine if self-assembly of small molecule amphiphiles within the solvent defects would change the motion of the defects driven by electric fields. BODIPY was used because it exhibits distinct changes in optical absorption and emission spectra before and after self-association<sup>61</sup> within the solvent defects at critical aggregation concentrations (CAC) determined by the tail-length (45 µM for BODIPY-C5, 35 µM for BODIPY-C12).46 When imaged using a fluorescence microscope, at concentrations above the CAC, bright lines were visible in the dimer channel (λ<sub>em</sub>: 606-684 nm;) at the location of the solvent defects (as seen by bright field imaging), consistent with selfassociation of the amphiphiles within the nanoscopic environment created by the defects but not in the bulk nematic solvent phase (Figure 2f). Following application of an AC electric field, we observed the dimer fluorescence generated by BODIPY-C12 assemblies to move with the location of the defect (confirmed by locating the defect using bright field microscopy) (Figure 2b-i). In comparison to the defect motion observed without BODIPY-C12, we found the presence of assemblies within defects to slow defect motion (Figure 2j). Specifically, we tracked the defect positions in the presence of BODIPY-C5 and BODIPY-C12 at two amphiphile concentrations and two applied voltages (see Supporting Information for plots of position as a function of time). We found that (i) the defect velocity increased with increasing voltage both in the absence and presence of assemblies and (ii) under similar applied voltage differences, the defect velocities decreased

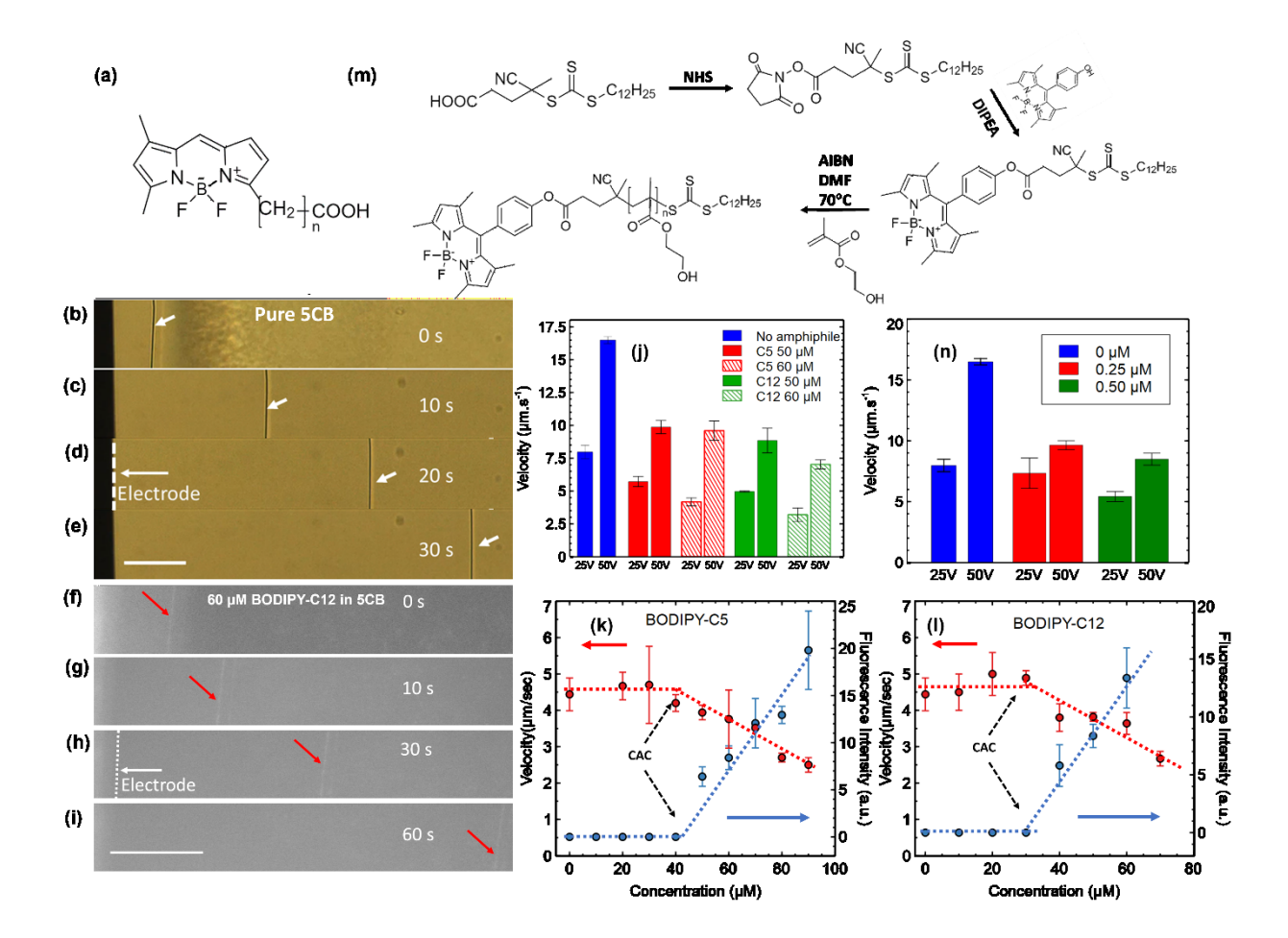


Figure 2. (a) Molecular structure of BODIPY-C<sub>n+1</sub>. (b-e) Bright-field micrographs of a line defect formed in a nematic solvent phase of 5CB, driven into motion by application of a voltage to the electrode on the left side of the image (50V). The electrode is denoted by the white dotted line in (d). The defects are imaged at the indicated times (following the application of the voltage). Scale bar, 100 µm. (f-i) Fluorescence micrographs showing displacement of BODIPY-C12 assemblies formed in the defects of nematic 5CB. The concentration of the BODIPY-C12 in the 5CB was 60 µm. The voltage was 50 V. The location of the electrode is denoted by the white dotted line in (h). Red arrows indicate location of assembly within the defect (bright dimer fluorescence signal). Scale bar, 100 µm. (j) Velocities of defects hosting assemblies formed from BODIPY-C12 and C5. The separation between electrodes was 3 mm in these experiments. (k-l) Velocities of assemblies formed in defects (fluorescence signals, shown in red circles) from (k) BODIPY-C5 and (1) BODIPY-C12 as a function of amphiphile concentration. The voltage was 25 V and the separation between electrodes was 3.3mm. The corresponding fluorescence intensities are shown in blue circles. Lines drawn to guide the eye. (m) Synthetic route of trithiocarbonate chain-transfer agent (BODIPY-CTA) and BODIPY-poly(HEMA). NHS is N-Hydroxysuccinimide, DIPEA is N,N-Diisopropylethylamine, AIBN is Azobisisobutyronitrile, and DMF is N,N-Dimethylformamide. (n) Velocities of defects hosting BODIPY-poly(HEMA) assemblies as a function of applied voltage. Contrast was enhanced in (f-i) to aid visualization of fluorescence signals

with increase in amphiphile concentration. For example, when applying 25 V (electric field – 8.3 V/mm), defects hosting the assemblies formed from 50  $\mu$ M BODIPY-C5 moved at velocities of 5.7  $\pm$  0.4  $\mu$ m·s<sup>-1</sup> while the corresponding velocity at 60  $\mu$ M was 4.2  $\pm$  0.3  $\mu$ m.s<sup>-1</sup>. Similarly, the velocities for 50  $\mu$ M and 60  $\mu$ M BODIPY-C12 were 5.0  $\pm$  0.04  $\mu$ m.s<sup>-1</sup> and 3.2  $\pm$  0.5  $\mu$ m.s<sup>-1</sup>, respectively. These results led us to hypothesize that the decrease in defect velocity with increasing amphiphile concentration reflects an increase in size of the assembly of molecules hosted in the defect.

Support for the above-described hypothesis can be found in the results of Figure 2k and 2l, where defect velocities measured at 25 V (electric field – 7.5 V/mm) are shown to decrease with increase in concentration above but not below the CAC of BODIPY-C12 and BODIPY-C5. The dimer fluorescence intensity from the defect, which correlates with size of the BODIPY assembly, increases with increase in concentration above the CAC.<sup>46</sup> When combined, we interpret these results to indicate that the size of an assembly formed within a defect impacts the drag on the defect.

Finally, when the voltage used to drive the defect motion was increased to 50 V (electric field: 16.6 V/mm), we also measured the defect velocity to decrease with increase in BODIPY-C12 concentration, although the dependence on amphiphile concentration and tail length was measured to be weaker at the higher voltage (see SI). These results suggest that the drag created by the assembly of molecules within the core of the defect may be less important in determining defect motion at high defect velocities. We hypothesize that dissipative contributions arising from far-field motion of the nematic solvent may dominate defect motion at high voltages and velocities. 60,62

Next, we performed experiments to determine if assemblies formed from polymers within defects of nematic solvents impact defect dynamics in ways that are similar to those reported above for small molecule amphiphiles. For these studies, we prepared poly(HEMA) end-labeled with BODIPY (BODIPY-poly(HEMA); see Figure 2m) which, as described in the Introduction, we have shown previously to form well-defined assemblies within defects.<sup>51</sup> Here, we focus on BODIPY-poly(HEMA) with degree of polymerization (DP) = 50 and concentrations of BODIPYpoly(HEMA) that exceed its CAC (0.2  $\mu$ M) in m = -1/2 defects of 5CB. Our measurements lead to two key conclusions. First, we found that assemblies of BODIPY-poly(HEMA) formed in the defects were transported by electric field-driven defect motion, and that defect velocities decreased with increasing concentration of polymer (at constant voltage) (Figure 2n, S6). These results are qualitatively similar to the results obtained with the small molecule amphiphiles (see Figure 2j), and consistent with a concentration-dependent growth in the size of the polymer assembly. Second, and more significantly, the magnitudes of the velocities measured with the BODIPY-poly(HEMA) are strikingly similar to BODIPY-C5/C12 (Figure S7), despite the fact that the concentrations of the polymer and amphiphile in the bulk nematic solvent differ by over two orders of magnitude. This similarity, however, mirrors the shared morphology (worm-like) and diameters ( $28 \pm 4$  nm for the amphiphiles<sup>46</sup> and  $30 \pm 5$  nm for the polymers.<sup>51</sup>) of the assemblies formed in the defects. Overall, this result provides further support for our conclusion that the dynamic response of the defect to the applied field correlates with the size of the assembly of molecules hosted within the defect. More broadly, measurements of the motion of defects hosting assemblies offers a promising approach to characterization of single assemblies of molecules (e.g., the CAC or the size of the assembly). We also performed experiments with a thinner film (200 µm) of 5CB, and observed that assemblies of small amphiphiles and polymers slow the defect movement (Fig S8).

Motivated by the goal of developing methods to transport reactants and products between distinct solvent environments (e.g., within integrated chemical systems), we next performed experiments to determine if we could transport assemblies of molecules between solvent regions containing different concentrations of amphiphile or polymer. To this end, we prepared nematic solvent domains with patterned concentrations of amphiphiles using the procedure depicted in Figure 3ac (See SI). Our first experiments using the set-up shown in Figure 3a-c were performed with 50 μM BODIPY-C12 (placed into the region indicated in green in Figure 3). Immediately after removal of the central wire and before application of a voltage, inspection of Figure 3e reveals that the left side of the micrograph exhibited a stronger dimer fluorescence signal than the right side of the image. This gradient in fluorescence signal arises from the initial confinement of BODIPY-C12 to the left side of the nematic solvent domain. The defect is visible as a bright line near the left side of the image in Figure 3e (see also Figure 3d for a bright field image of the defect). The gradient in concentration of BODIPY-C12 evident in Figure 3e is long-lived on the time-scale of our experiment (mins). We estimated the diffusion length of BODIPY-C12 after 100 s to be 5  $\mu$ m (assuming D  $\approx 1 \, \mu m^2/s$ )<sup>63</sup> which is one order of magnitude smaller than the distance over which we observed the variation in the fluorescence signal (~ 100 μm) in Figure 3e. This observation also indicates that the initial concentration profile of the BODIPY-C12 is influenced by convection induced during removal of the wire. Following application of the voltage (25 V), we observed the defect shown in Figure 3e to be driven out of the region of the nematic solvent containing the high concentration of BODIPY-C12 approximately 45 s after the onset of the voltage (Figure 3e-m). We quantified the fluorescence intensity of the BODIPY-C12 assembly during the displacement of the defect across the sample (Figure 3o).

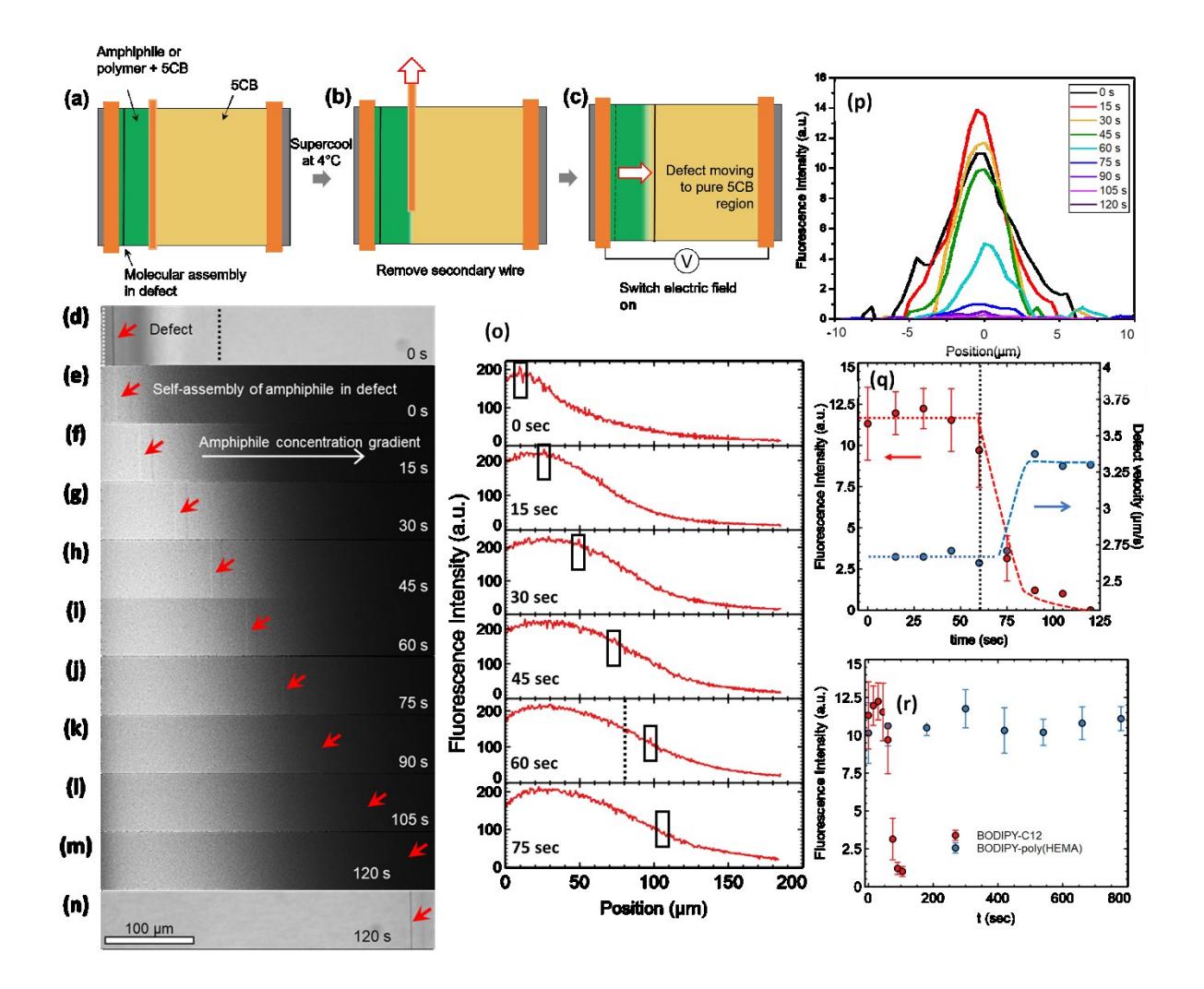


Figure 3. (a) Schematic illustration of nematic solvent either containing amphiphile (green) or free of amphiphile (yellow). The two solvent regions are initially separated by a metallic wire within an optical cell. A defect, shown to form adjacent to the wire (electrode) on the left, hosts an assembly formed from the amphiphile present in the nematic solvent. (b) Removal of the wire generates a concentration gradient of amphiphile. (c) Upon application of a voltage, the defect hosting the amphiphilic assembly moves down the concentration gradient towards the amphiphile-free region of the nematic solvent. (d) Bright field micrographs showing the location of a topological defect (m = -1/2) in a nematic solvent phase. The dotted line in (d) indicates the location of the secondary wire prior to removal. (e-n) Fluorescence micrographs showing dimer fluorescence moving with the defect as a function of time under an applied voltage. Time indicates the time after the voltage was applied (25V, 1kHz AC, 50µM BODIPY-C12). Contrast was enhanced in these images to aid the visualization of defect. (o) Fluorescence intensity measured and averaged in regions (380 μm ×180 μm) within the sample as a function of time. Peaks in fluorescence signal correspond to the location of assemblies, and are enclosed in black rectangles, position = 0 corresponds to the electrode surface. (p) Fluorescence from amphiphiles hosted in defects, after subtraction of base line intensity, as a function of time following the application of the voltage. (q) Velocity of defects containing amphiphile

assemblies as a function of time following the application of voltage (shown in blue). The corresponding fluorescence intensity of the assemblies are shown in red. (r) Fluorescence intensity from BODIPY-labeled fatty acid (red data) or BODIPY- poly(HEMA) (blue data) assemblies formed in defects in nematic 5CB, plotted as a function of time during displacement of the defect across the optical cells illustrated in (d-n). (25V, 1kHz AC, 50µM BODIPY-C12, 50V, 1kHz AC, 0.5µM BODIPY-poly(HEMA).

Following subtraction of the baseline intensity, we obtained the plots shown in Figure 3p. Inspection of Figure 3p reveals that for times between 0 and 45 s (during which time the defect traversed the amphiphile-rich region), the fluorescence intensity of the BODIPY-C12 assembly was largely invariant. The small increase in fluorescence intensity in the first 30 seconds (approximately 18% and 9% at 15s and 30s) lies within the uncertainty of the measurement (Figure 3r). Upon moving into the nematic solvent region that was largely free of amphiphile (low fluorescence intensity), we recorded a pronounced decrease in the intensity of the fluorescence signal from the BODIPY-C12 assembly in the defect (Figure 3p). This decrease in fluorescence signal, in a region of amphiphile concentration below the CAC (the estimated position of the CAC is indicated by the dotted black line in Figure 30 – 60s panel), indicates disassembly of the BODIPY-C12 from the core of the solvent defect. We estimated the lifetime of the assembly in the region of solvent containing an amphiphile concentration below the CAC to be 14s (See SI, Figure S12). Since the lifetime of the assembly is less than the time required to relocate the defect from a region of high amphiphile concentration to low amphiphile concentration (~45 s), we also conclude that assemblies within the defect undergo dynamic exchange with the bulk solution as the defect traverses the optical cell during the first 45s in our experiment. Specifically, we estimate that it is possible to displace a given BODIPY-12 assembly by approximately 45 µm (velocity x lifetime, velocity  $\sim 3.3 \ \mu m.s^{-1}$ , lifetime  $\sim 14 \ s$ ) before the amphiphiles within the assembly are exchanged with amphiphiles present in the bulk nematic solvent. Overall, the rapid exchange of amphiphiles between the defect and the bulk of the nematic solvent that is evident in Figure 3 leads

us to conclude that defect-templated self-assembled structures formed by BODIPY-C12 are kinetically labile and are transported via transient association with the moving defect (Figure S16).

We make one additional observation regarding the results in Figure 3e-m. Along with displacement of the position of the defect, Figure 3e-m shows that the intensity of the fluorescence signal from the BODIPY-amphiphiles dissolved in the bulk of the nematic solvent increased upon application of the voltage (compare Figure 3e to 3g). We confirmed that the application of the electric field did not cause migration of the amphiphiles in the absence of defects and that the increase in fluorescence intensity arises from the reorientation of the nematic solvent. This interpretation is supported by observations made with BODIPY amphiphiles in cells with uniform concentrations (Figure S11).

Next, we performed experiments of the type described in Figure 3o-p using BODIPY-poly(HEMA) (see SI for details). Quantification of the fluorescence intensity, as a function of time, is shown in Figures S13 and S14 and summarized in Figure 3r. Inspection of Figure 3r reveals that, in contrast to BODIPY-C12, the fluorescence signal from BODIPY-poly(HEMA) did not decay when the assembly was transported into a region of nematic solvent that contained a concentration of BODIPY-poly(HEMA) below the CAC. Specifically, the fluorescence intensity of the BODIPY-poly(HEMA) assembly was unchanged after 20 minutes of equilibration in polymer-free nematic solvent (Figure 3r). Experiments performed with a higher concentration (0.6 μM) of BODIPY-poly(HEMA) also revealed similar results (Figure S15). We interpret this overall behavior, which contrasts to BODIPY-C12, to reflect slow disassembly kinetics of BODIPY-poly(HEMA) in the defects of nematic 5CB. We also note that assemblies of BODIPY-poly(HEMA), when transported to regions below the CAC, are not permanent but dissociate after approximately 24 hours. Additionally, we have also observed that upon heating the nematic 5CB

to form an isotropic solvent phase, a process that eliminates the solvent defects, BODIPY-poly(HEMA) assemblies present initially within a defect dissociate after a period of ~ 24 hours. <sup>51</sup> These results lead us to conclude that, in contrast to small amphiphiles, polymers like BODIPY-poly(HEMA) form long-lived, but not permanent, self-assembled structures within defects of nematic phases of 5CB. It also provides support for our conclusion that electric-field induced defect movement leads to the transport of a single polymeric assembly across the entire LC sample during displacement of the host defect (Figure S16).

We exploited the long lifetimes of the polymeric assemblies in defects to demonstrate that defects in nematic solvents can be used to "collect" and "store" macromolecular cargo. For these experiments, we filled the region between the primary and secondary wires shown in Figure 3a with pure 5CB, while the remaining volume of the optical cell was filled with 5CB + 0.3 μM BODIPY- poly(HEMA). Using an applied voltage, we repositioned the defect present initially in the polymer-free region of the nematic phase into the polymer-rich zone within which it triggered formation of a polymeric assembly (Figure 4a-l). Using this approach, we were able to study the dynamics of formation of the polymer assembly within the defect. Figure S17 shows that the

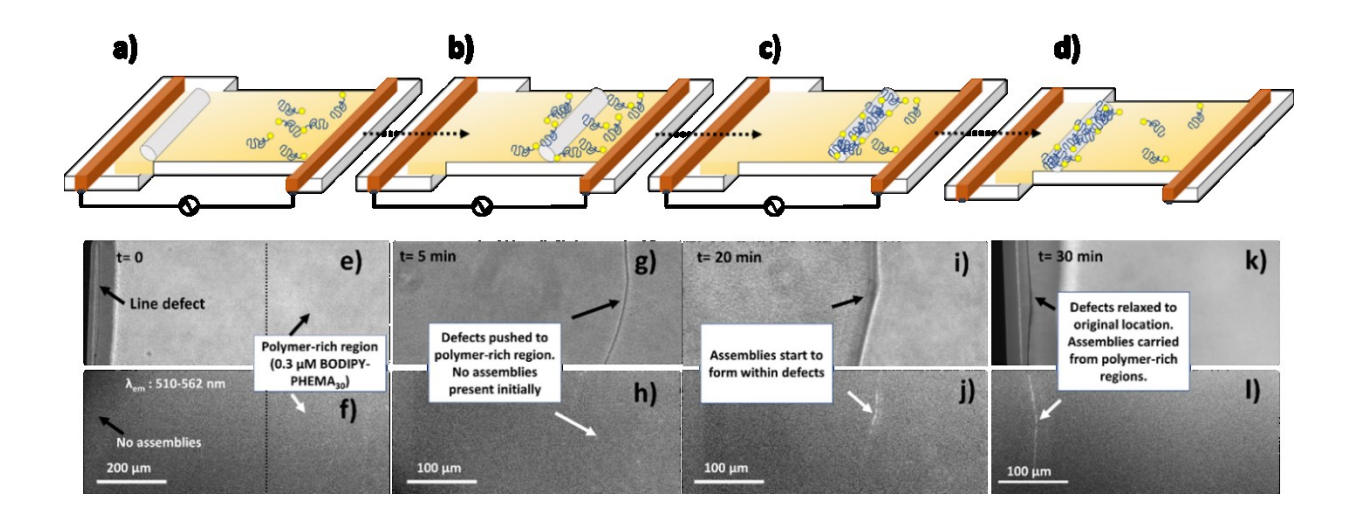


Figure 4. (a-d) Schematic illustration of defects used as vehicles to carry molecular cargo from a polymer-rich region of 5CB to polymer-lean region of solvent. (e) Bright field and (f) fluorescence images of assembly-free defect present initially in the polymer-free region of solvent. The dotted line in (e) and (f) indicates the location of the transition from polymer-free to polymer-rich solvent. (g, h) Defect is repositioned using an electric field to a region of solvent containing 0.3 µM BODIPY-poly(HEMA) (50V, 1kHz). No assemblies are present initially within the defects. (i, j) Bright field and fluorescence images showing formation of assemblies within the defects after 20 minutes. (k) The defect, carrying molecular cargo, returns to its initial location once electric field is turned off. (l) Fluorescence image showing that the defect carries the polymeric assemblies along with into the polymer-lean region.

assemblies start to form within approximately 10 minutes of arrival of the defect in the polymer-rich region of the solvent. The assembly-loaded defect was then returned to the polymer-free region by removing the applied voltage (Figure 4k-l). Overall, this process resulted in the programmed formation of a polymeric assembly (triggered to form by the electric-field driven displacement of the defect), and its repositioning into a polymer-free region of solvent. These results provide further evidence of the potential utility of defects as programmable carriers and nanoreactors based on molecular self-assembly within their nanoscopic cores.

This paper reports several key advances related to the formation and manipulation of single assemblies of molecules. Our strategy exploits geometry-induced defects in nematic solvents to enable formation of a single assembly of molecules at a predictable location within the solvent. This capability contrasts to molecular assembly in isotropic solvents (e.g., water), where multiple assemblies form at random locations within the solvent. Specifically, we reveal for the first time how electric field-driven defect motion in nematic solvents is influenced by the presence of amphiphilic or polymer assemblies hosted in the defects. Our observations identify the importance of assembly size in determining the drag acting on the defects during their motion, particularly at low defect velocities, thus providing an approach to characterization of the properties (e.g., sizes) of single assemblies of molecules formed in defects. In addition, our results also suggest that it may be possible to develop molecular separation processes based on differential rates of motion

of defects. Such separation and analysis processes could find use in nanoscale reactor networks where assemblies formed in defects are used as nanocontainers for chemical synthesis.

In addition, our work provides the first evidence of the use of defects as programmable vehicles for moving molecular cargo (Figure 4b-d), including the use of defects to transport assemblies between regions of solvent that possess distinct compositions. In doing so, we characterize the dynamics of molecular assembly and disassembly within defects. We envisage future studies in which assemblies are moved into solvent regions containing reactive species that partition into the assemblies and undergo reaction. In particular, our data show that polymeric assemblies can be sufficiently long-lived that they offer the basis of nanocontainers suitable for use during chemical synthesis (e.g., a reaction involving the polymer). Additionally, we point out that the distances over which the defects can be moved on time scales of minutes are far greater than diffusion distances of even small solutes, thus permitting compositional differences in a given solvent volume to be maintained during syntheses in which the defect is moved between various solvent regions (compositions). This observation reinforces our proposal that molecular assemblies hosted in topological defects offer exciting opportunities for integrated chemical systems.

Our results also highlight several future directions of research. For example, our data suggest that there is a complex interplay of near-core and far-field solvent dynamics that determine the effective drag on a molecular assembly hosted within a defect. Additionally, our current understanding of the nanostructures formed by amphiphiles and polymers within defects in nematic solvents comes from equilibrium studies. It is possible that the motion of the defect driven by an electric field may change those nanostructures. Indeed, moving forward, *in-situ* liquid-phase transmission electron microscopy (LPTEM)<sup>64-66</sup> may provide one approach to the characterization of the morphological changes induced by defect motion.

**Acknowledgements** This research was primarily supported by the Army Research Office (W911NF-15-1-0568 and W911NF-19-1-0071), with additional support from the National Science Foundation (CBET-1803409 and CBET-1852379). The use of the shared facilities of the Cornell Center for Materials Research (MRSEC DMR-1719875) is acknowledged. Northwestern University Integrated Molecular Structure Education and Research Center (IMSERC) is acknowledged.

## **Supporting Information.**

- 1. Synthesis and characterization of BODIPY-poly(HEMA)
- 2. Defect displacements and velocities for BODIPY-C5, C12 and BODIPY-poly(HEMA) at different voltages.
- 3. Fluorescence intensities as a function of time in cells with uniform and patterned amphiphile concentrations.
- 4. Schematic illustration of the mechanism of amphiphile/polymer exchange

The following files are available free of charge.

Supporting Information.pdf

## **Corresponding Author**

\*nabbott@cornell.edu

\*nathan.gianneschi@northwestern.edu

## **Author Contributions**

The manuscript was written through contributions of all authors. All authors have given approval to the final version of the manuscript. ‡These authors contributed equally.

## REFERENCES

- (1) Wang, T.; Oehrlein, S.; Somoza, M. M.; Sanchez Perez, J. R.; Kershner, R.; Cerrina, F. Optical Tweezers Directed One-Bead One-Sequence Synthesis of Oligonucleotides. *Lab Chip* 2011, 11 (9), 1629–1637.
- (2) Brás, E. J. S.; Domingues, C.; Chu, V.; Fernandes, P.; Conde, J. P. Microfluidic Bioreactors for Enzymatic Synthesis in Packed-Bed Reactors—Multi-Step Reactions and Upscaling. *J. Biotechnol.* **2020**, *323*, 24–32.
- (3) Penny, M. R.; Hilton, S. T. Design and Development of 3D Printed Catalytically-Active Stirrers for Chemical Synthesis. *React. Chem. Eng.* **2020**, *5* (5), 853–858.
- (4) Mawatari, K.; Kazoe, Y.; Aota, A.; Tsukahara, T.; Sato, K.; Kitamori, T. Microflow Systems for Chemical Synthesis and Analysis: Approaches to Full Integration of Chemical Process. *J. Flow Chem.* **2012**, *1* (1), 3–12.
- (5) Balbino, T. A.; Serafin, J. M.; Radaic, A.; de Jesus, M. B.; de la Torre, L. G. Integrated Microfluidic Devices for the Synthesis of Nanoscale Liposomes and Lipoplexes. *Colloids Surfaces B Biointerfaces* **2017**, *152*, 406–413.
- (6) Leibfarth, F. A.; Johnson, J. A.; Jamison, T. F. Scalable Synthesis of Sequence-Defined, Unimolecular Macromolecules by Flow-IEG. *Proc. Natl. Acad. Sci. U. S. A.* 2015, 112 (34), 10617–10622.
- (7) Easley, C. J.; Karlinsey, J. M.; Bienvenue, J. M.; Legendre, L. A.; Roper, M. G.; Feldman, S. H.; Hughes, M. A.; Hewlett, E. L.; Merkel, T. J.; Ferrance, J. P.; Landers, J. P. A Fully Integrated Microfluidic Genetic Analysis System with Sample-in–Answer-out Capability.

- Proc. Natl. Acad. Sci. 2006, 103 (51), 19272–19277.
- (8) Lim, J. M.; Bertrand, N.; Valencia, P. M.; Rhee, M.; Langer, R.; Jon, S.; Farokhzad, O. C.; Karnik, R. Parallel Microfluidic Synthesis of Size-Tunable Polymeric Nanoparticles Using 3D Flow Focusing towards in Vivo Study. *Nanomedicine Nanotechnology, Biol. Med.* 2014, 10 (2), 401–409.
- (9) Valencia, P. M.; Pridgen, E. M.; Rhee, M.; Langer, R.; Farokhzad, O. C.; Karnik, R. Microfluidic Platform for Combinatorial Synthesis and Optimization of Targeted Nanoparticles for Cancer Therapy. ACS Nano 2013, 7 (12), 10671–10680.
- (10) Castillo-León, J.; Castillo-León, J. Microfluidics and Lab-on-a-Chip Devices: History and Challenges. *Lab-on-a-Chip Devices Micro-Total Anal. Syst.* **2015**, 1–15.
- (11) Mohammed, M. I.; Haswell, S.; Gibson, I. Lab-on-a-Chip or Chip-in-a-Lab: Challenges of Commercialization Lost in Translation. *Procedia Technol.* **2015**, *20*, 54–59.
- (12) Rubio-Sánchez, R.; Barker, S. E.; Walczak, M.; Cicuta, P.; Michele, L. Di. A Modular, Dynamic, DNA-Based Platform for Regulating Cargo Distribution and Transport between Lipid Domains. *Nano Lett.* 2021, 21 (7), 2800–2808.
- (13) Fernandez-Trillo, F.; Grover, L. M.; Stephenson-Brown, A.; Harrison, P.; Mendes, P. M. Vesicles in Nature and the Laboratory: Elucidation of Their Biological Properties and Synthesis of Increasingly Complex Synthetic Vesicles. *Angew. Chemie Int. Ed.* 2017, 56 (12), 3142–3160.
- (14) Bolinger, P. Y.; Stamou, D.; Vogel, H. Integrated Nanoreactor Systems: Triggering the Release and Mixing of Compounds Inside Single Vesicles. J. Am. Chem. Soc. 2004, 126 (28), 8594–8595.
- (15) Breitenkamp, K.; Emrick, T. Novel Polymer Capsules from Amphiphilic Graft Copolymers

- and Cross-Metathesis. J. Am. Chem. Soc. 2003, 125 (40), 12070–12071.
- (16) Bae, J.; Lawrence, J.; Miesch, C.; Ribbe, A.; Li, W.; Emrick, T.; Zhu, J.; Hayward, R. C. Multifunctional Nanoparticle-Loaded Spherical and Wormlike Micelles Formed by Interfacial Instabilities. *Adv. Mater.* 2012, 24 (20), 2735–2741.
- (17) Tanner, P.; Baumann, P.; Enea, R.; Onaca, O.; Palivan, C.; Meier, W. Polymeric Vesicles: From Drug Carriers to Nanoreactors and Artificial Organelles. Acc. Chem. Res. 2011, 44 (10), 1039–1049.
- (18) Gaitzsch, J.; Huang, X.; Voit, B. Engineering Functional Polymer Capsules toward Smart Nanoreactors. *Chem. Rev.* **2015**, *116* (3), 1053–1093.
- (19) Gao, J.; Zhao, B.; Wang, M.; Serrano, M. A. C.; Zhuang, J.; Ray, M.; Rotello, V. M.; Vachet, R. W.; Thayumanavan, S. Supramolecular Assemblies for Transporting Proteins Across an Immiscible Solvent Interface. *J. Am. Chem. Soc.* 2018, 140 (7), 2421–2425.
- (20) Van Dongen, S. F. M.; Nallani, M.; Cornelissen, J. J. L. M.; Nolte, R. J. M.; Van Hest, J. C. M. A Three-Enzyme Cascade Reaction through Positional Assembly of Enzymes in a Polymersome Nanoreactor. *Chem. A Eur. J.* 2009, *15* (5), 1107–1114.
- (21) Peters, R. J. R. W.; Marguet, M.; Marais, S.; Fraaije, M. W.; Van Hest, J. C. M.; Lecommandoux, S. Cascade Reactions in Multicompartmentalized Polymersomes. *Angew. Chemie Int. Ed.* **2014**, *53* (1), 146–150.
- (22) Tan, J.; Huang, C.; Liu, D.; Li, X.; He, J.; Xu, Q.; Zhang, L. Polymerization-Induced Self-Assembly of Homopolymer and Diblock Copolymer: A Facile Approach for Preparing Polymer Nano-Objects with Higher-Order Morphologies. ACS Macro Lett. 2017, 6 (3), 298–303.
- (23) Shi, X.; Shen, M.; Möhwald, H. Polyelectrolyte Multilayer Nanoreactors toward the

- Synthesis of Diverse Nanostructured Materials. *Prog. Polym. Sci.* **2004**, *29* (10), 987–1019.
- (24) Thiele, M. J.; Davari, M. D.; Hofmann, I.; König, M.; Lopez, C. G.; Vojcic, L.; Richtering, W.; Schwaneberg, U.; Tsarkova, L. A. Enzyme-Compatible Dynamic Nanoreactors from Electrostatically Bridged Like-Charged Surfactants and Polyelectrolytes. *Angew. Chemie* 2018, 130 (30), 9546–9551.
- (25) Renggli, K.; Baumann, P.; Langowska, K.; Onaca, O.; Bruns, N.; Meier, W. Selective and Responsive Nanoreactors. *Adv. Funct. Mater.* **2011**, *21* (7), 1241–1259.
- (26) Trantidou, T.; Friddin, M.; Elani, Y.; Brooks, N. J.; Law, R. V.; Seddon, J. M.; Ces, O. Engineering Compartmentalized Biomimetic Micro- and Nanocontainers. ACS Nano 2017, 11 (7), 6549–6565.
- (27) Wang, X.; Feng, J.; Bai, Y.; Zhang, Q.; Yin, Y. Synthesis, Properties, and Applications of Hollow Micro-/Nanostructures. *Chem. Rev.* **2016**, *116* (18), 10983–11060.
- (28) Li, J.; Li, Y.; Wang, Y.; Ke, W.; Chen, W.; Wang, W.; Ge, Z. Polymer Prodrug-Based Nanoreactors Activated by Tumor Acidity for Orchestrated Oxidation/Chemotherapy. *Nano Lett.* **2017**, *17* (11), 6983–6990.
- (29) Helms, B.; Liang, C. O.; Hawker, C. J.; Fréchet, J. M. J. Effects of Polymer Architecture and Nanoenvironment in Acylation Reactions Employing Dendritic (Dialkylamino)Pyridine Catalysts. *Macromolecules* **2005**, *38* (13), 5411–5415.
- (30) Comellas-Aragonès, M.; Engelkamp, H.; Claessen, V. I.; Sommerdijk, N. A. J. M.; Rowan, A. E.; Christianen, P. C. M.; Maan, J. C.; Verduin, B. J. M.; Cornelissen, J. J. L. M.; Nolte, R. J. M. A Virus-Based Single-Enzyme Nanoreactor. *Nat. Nanotechnol.* 2007 210 2007, 2 (10), 635–639.
- (31) Lin, L.; Wang, M.; Peng, X.; Lissek, E. N.; Mao, Z.; Scarabelli, L.; Adkins, E.; Coskun, S.;

- Unalan, H. E.; Korgel, B. A.; Liz-Marzán, L. M.; Florin, E. L.; Zheng, Y. Opto-Thermoelectric Nanotweezers. *Nat. Photonics* 2018 124 2018, 12 (4), 195–201.
- (32) Hill, E. H.; Li, J.; Lin, L.; Liu, Y.; Zheng, Y. Opto-Thermophoretic Attraction, Trapping, and Dynamic Manipulation of Lipid Vesicles. *Langmuir* **2018**, *34* (44), 13252–13262.
- (33) Yoshino, T.; Yamaura, D.; Komiya, M.; Sugawara, M.; Mitsumori, Y.; Niwano, M.; Hirano-Iwata, A.; Edamatsu, K.; Sadgrove, M. Optical Transport of Sub-Micron Lipid Vesicles along a Nanofiber. *Opt. Express* **2020**, *28* (26), 38527–38538.
- (34) Marchetti, M.; Kamsma, D.; Cazares Vargas, E.; Hernandez García, A.; Van Der Schoot, P.; De Vries, R.; Wuite, G. J. L.; Roos, W. H. Real-Time Assembly of Viruslike Nucleocapsids Elucidated at the Single-Particle Level. *Nano Lett.* 2019, 19 (8), 5746–5753.
- (35) Powers, A. S.; Liao, H. G.; Raja, S. N.; Bronstein, N. D.; Paul Alivisatos, A.; Zheng, H. Tracking Nanoparticle Diffusion and Interaction during Self-Assembly in a Liquid Cell. *Nano Lett.* **2017**, *17* (1), 15–20.
- (36) Galan, E. A.; Zhao, H.; Wang, X.; Dai, Q.; Huck, W. T. S.; Ma, S. Intelligent Microfluidics: The Convergence of Machine Learning and Microfluidics in Materials Science and Biomedicine. *Matter* **2020**, *3* (6), 1893–1922.
- (37) Rizzuto, V.; Mencattini, A.; Álvarez-González, B.; Di Giuseppe, D.; Martinelli, E.; Beneitez-Pastor, D.; Mañú-Pereira, M. del M.; Lopez-Martinez, M. J.; Samitier, J. Combining Microfluidics with Machine Learning Algorithms for RBC Classification in Rare Hereditary Hemolytic Anemia. *Sci. Reports* 2021 111 2021, 11 (1), 1–12.
- (38) Epps, R. W.; Abolhasani, M. Modern Nanoscience: Convergence of AI, Robotics, and Colloidal Synthesis. *Appl. Phys. Rev.* **2021**, *8* (4), 041316.
- (39) Tao, H.; Wu, T.; Kheiri, S.; Aldeghi, M.; Aspuru-Guzik, A.; Kumacheva, E.; Tao, H.; Wu,

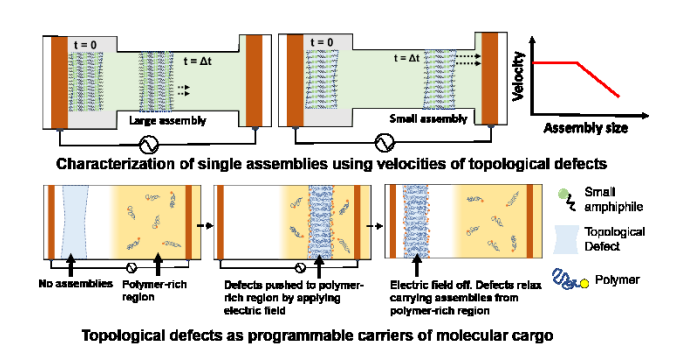
- T.; Aldeghi, M.; Aspuru-Guzik, A.; Kumacheva, E.; Kheiri, S. Self-Driving Platform for Metal Nanoparticle Synthesis: Combining Microfluidics and Machine Learning. *Adv. Funct. Mater.* **2021**, 2106725.
- (40) Atanase, L.; Riess, G. Self-Assembly of Block and Graft Copolymers in Organic Solvents:

  An Overview of Recent Advances. *Polymers (Basel)*. **2018**, *10* (1), 62.
- (41) Corradi, E.; Meille, S. V.; Messina, M. T.; Metrangolo, P.; Resnati, G. Halogen Bonding versus Hydrogen Bonding in Driving Self-Assembly Processes. *Angew. Chemie Int. Ed.* **2000**, *39* (10), 1782–1786.
- (42) Priimagi, A.; Cavallo, G.; Forni, A.; Gorynsztejn-Leben, M.; Kaivola, M.; Metrangolo, P.; Milani, R.; Shishido, A.; Pilati, T.; Resnati, G.; Terraneo, G. Halogen Bonding versus Hydrogen Bonding in Driving Self-Assembly and Performance of Light-Responsive Supramolecular Polymers. *Adv. Funct. Mater.* **2012**, *22* (12), 2572–2579.
- (43) He, Y.; Li, Z.; Simone, P.; Lodge, T. P. Self-Assembly of Block Copolymer Micelles in an Ionic Liquid. *J. Am. Chem. Soc.* **2006**, *128* (8), 2745–2750.
- (44) Greaves, T. L.; Drummond, C. J. Ionic Liquids as Amphiphile Self-Assembly Media. *Chem. Soc. Rev.* **2008**, *37* (8), 1709–1726.
- (45) de Gennes, Pierre-Gilles; Prost, J. *The Physics of Liquid Crystals*; Oxford University Press, 1993.
- (46) Wang, X.; Miller, D. S.; Bukusoglu, E.; De Pablo, J. J.; Abbott, N. L. Topological Defects in Liquid Crystals as Templates for Molecular Self-Assembly. *Nat. Mater.* **2016**, *15* (1), 106–112.
- (47) Wang, X.; Kim, Y. K.; Bukusoglu, E.; Zhang, B.; Miller, D. S.; Abbott, N. L. Experimental Insights into the Nanostructure of the Cores of Topological Defects in Liquid Crystals. *Phys.*

- Rev. Lett. 2016, 116 (14), 147801.
- (48) Lin, I. H.; Miller, D. S.; Bertics, P. J.; Murphy, C. J.; De Pablo, J. J.; Abbott, N. L. Endotoxin-Induced Structural Transformations in Liquid Crystalline Droplets. *Science* (80-.). 2011, 332 (6035), 1297–1300.
- (49) Miller, D. S.; Abbott, N. L. Influence of Droplet Size, PH and Ionic Strength on Endotoxin-Triggered Ordering Transitions in Liquid Crystalline Droplets. *Soft Matter* **2013**, *9* (2), 374–382.
- (50) Milette, J.; Relaix, S.; Lavigne, C.; Toader, V.; Cowling, S. J.; Saez, I. M.; Lennox, R. B.; Goodby, J. W.; Reven, L. Reversible Long-Range Patterning of Gold Nanoparticles by Smectic Liquid Crystals. *Soft Matter* 2012, 8 (24), 6593–6598.
- (51) Noh, J.; Cao, W.; Sun, H.; Yang, Y.; Gianneschi, N. C.; Abbott, N. L. Self-Assembly of Macromolecules Within Single Topological Defects of Nematic Solvents. *Chem. Mater.* 2020, 32 (15), 6753–6764.
- (52) Kleman, M.; Lavrentovich, O. D. Topological Point Defects in Nematic Liquid Crystals. *Philos. Mag.* **2006**, *86* (25–26), 4117–4137.
- (53) Mottram, N. J.; Sluckin, T. J. Defect-Induced Melting in Nematic Liquid Crystals. *Liq. Cryst.* **2000**, *27* (10), 1301–1304.
- (54) Fleury, B.; Senyuk, B.; Tasinkevych, M.; Smalyukh, I. I. Interplay of Electrostatic Dipoles and Monopoles with Elastic Interactions in Nematic Liquid Crystal Nanocolloids. *Nano Lett.* **2020**, *20* (11), 7835–7843.
- (55) Ranganath, G. S. Defect States in a Nematic Liquid Crystal in a Magnetic Field. *Mol. Cryst. Liq. Cryst. Inc. Nonlinear Opt.* **1988**, *154* (1), 43–53.
- (56) Terentjev, E. M. Disclination Loops, Standing Alone and around Solid Particles, in Nematic

- Liquid Crystals. Phys. Rev. E 1995, 51 (2), 1330–1337.
- (57) O'Rourke, M. J. E.; Ding, D. K.; Thomas, E. L.; Percec, V. Morphologies and Energies of Néel Inversion Wall Defects in a Liquid Crystal Polyether. *Macromolecules* 2001, 34 (19), 6658–6669.
- (58) Velez, J. X.; Zheng, Z.; Beller, D. A.; Serra, F. Emergence and Stabilization of Transient Twisted Defect Structures in Confined Achiral Liquid Crystals at a Phase Transition. *Soft Matter* **2021**, *17* (14), 3848–3854.
- (59) Jiang, J.; Ranabhat, K.; Wang, X.; Rich, H.; Zhang, R.; Peng, C. Active Transformations of Topological Structures in Light-Driven Nematic Disclination Networks. *Proc. Natl. Acad.* Sci. 2022, 119 (23), e2122226119.
- (60) Cladis, P. E.; Van Saarloos, W.; Finn, P. L.; Kortan, A. R. Dynamics of Line Defects in Nematic Liquid Crystals. *Phys. Rev. Lett.* **1987**, *58* (3), 222–225.
- (61) Mikhalyov, I.; Gretskaya, N.; Bergström, F.; Johansson, L. B. . Electronic Ground and Excited State Properties of Dipyrrometheneboron Difluoride (BODIPY): Dimers with Application to Biosciences. *Phys. Chem. Chem. Phys.* 2002, 4 (22), 5663–5670.
- (62) Tóth, G.; Denniston, C.; Yeomans, J. M. Hydrodynamics of Topological Defects in Nematic Liquid Crystals. *Phys. Rev. Lett.* **2002**, *88* (10), 105504.
- (63) Kolahi, K.; Louey, S.; Varlamov, O.; Thornburg, K. Real-Time Tracking of BODIPY-C12 Long-Chain Fatty Acid in Human Term Placenta Reveals Unique Lipid Dynamics in Cytotrophoblast Cells. *PLoS One* 2016, 11 (4), e0153522.
- (64) De Yoreo, J. J.; N. A. J. M., S. Investigating Materials Formation with Liquid-Phase and Cryogenic TEM. *Nat. Rev. Mater.* **2016**, *I* (8), 16035.
- (65) Touve, M. A.; Carlini, A. S.; Gianneschi, N. C. Self-Assembling Peptides Imaged by

- Correlated Liquid Cell Transmission Electron Microscopy and MALDI-Imaging Mass Spectrometry. *Nat. Commun.* **2019**, *10* (1), 4837.
- Touve, M. A.; Figg, C. A.; Wright, D. B.; Park, C.; Cantlon, J.; Sumerlin, B. S.; Gianneschi,
   N. C. Polymerization-Induced Self-Assembly of Micelles Observed by Liquid Cell
   Transmission Electron Microscopy. ACS Cent. Sci. 2018, 4 (5), 543–547.



TOC Graphic